Low Density Plasma Waveguides Driven by Ultrashort (30 fs) and Long (300 ps) Pulses for Laser Wakefield Acceleration

Isabella Pagano
Department of Physics
University of Texas at Austin
Austin, USA
ipagano@utexas.edu

Jarrod Leddy Tech-X Corporation Boulder, USA jleddy@txcorp.com Jason Brooks

Department of Physics

University of Texas at Austin

Austin, USA
jasonbrooks@utexas.edu

John Cary
Department of Physics
University of Colorado
Boulder, USA
Tech-X Corporation
Boulder, USA
cary@colorado.edu

Aaron Bernstein
Department of Physics
University of Texas at Austin
Austin, USA
abernste@mail.utexas.edu

Michael C. Downer

Department of Physics

University of Texas at Austin

Austin, USA

downer@physics.utexas.edu

Rafal Zgadzaj

Department of Physics

University of Texas at Austin

Austin, USA

rafal@physics.utexas.edu

Abstract—We simulate the possibility of scaling channel formation to low densities plasmas of low atomic number gas over a large range of pulse duration including (1) pulses up to 300 ps in duration, using inverse bremsstrahlung (IB) heating and (2) ultrashort pulses up to 100s of femtoseconds for generating tenuous plasmas of centimeter to meter lengths by optical field ionization (OFI) [1]. Results show IB heating up to tens of eV, and channels formed from an initial density of $1\times10^{18}~{\rm cm}^{-3}$ with axial densities as low as $1\times10^{17}~{\rm cm}^{-3}$, and radius of 50 μm . It has been shown that centimeter-scale waveguides can be generated via OFI heating at densities of approximately $1\times10^{17}~{\rm cm}^{-3}$ [2]; we show calculations and theory of this channel formation using an axicon. Lastly, we outline the experimental setup to be used in future experiments at the University of Texas Tabletop Terawatt (UT3) facility.

Keywords—laser stability, optical waveguides, plasma accelerators

I. INTRODUCTION

One of the challenges to producing tens-of-GeV electrons from a single-stage laser plasma accelerator is a meter-scale cylindrical waveguide made of low-density ($n_e < 10^{18} \ {\rm cm}^{-3}$), fully-ionized low-Z plasma. Plasma waveguides improve shot-to-shot consistency of laser wakefield accelerators (LWFAs) and extend acceleration lengths to multiple Rayleigh ranges. In the 1990s, line-focused 0.5 J, and 100 ps laser pulses were used to ionize atmospheric density, high-atomic number (Z) gases, and to heat the resulting plasma (n_e greater than $3 \times 10^{18} \ {\rm cm}^{-3}$) to approximately 50 eV via inverse bremsstrahlung (IB), launching a cylindrical blastwave that formed a plasma waveguide [3], [4]. However, with available lasers at the

The software used in this work was in part developed by the DOE NNSA-ASC OASCR Flash Center at the University of Chicago. This work was supported by U.S. National Science Foundation grant PHY1734319 and U.S. DoE grant DE-SC0011617

time, IB heating became too inefficient to form waveguides in low-Z, low-density plasma. Because of now available and technologically advanced laser systems, including the Texas Petawatt, we can utilize IB heating with parameters not possible on previous systems. Simulations, using a particlein-cell code, assume an ionizing/heating pulse of 800 nm wavelength, 1-2 J energy, pulse duration variable from a few to several hundred picoseconds, and a line-focus of millimeter to centimeter lengths, matching parameters of the University of Texas Tabletop Terawatt (UT3) facility. The target is 10-100 Torr He gas, with optional high-Z dopants. In contrast to IB heating, optical field ionization (OFI) heating can be driven by femtosecond, rather than picosecond pulses, is nearly independent of gas density, and can heat selected plasma species to tens of eV electron temperature at densities n_e less than 10^{18} cm⁻³. We find that gas species with higher atomic number yield hotter plasmas, but are difficult to ionize fully for Z greater than 2. He gas (Z=2) is therefore a promising candidate for low-density OFI waveguide formation. We study how blastwave formation varies from an axicon beam.

II. INVERSE BREMSSTRAHLUNG HEATING

Inverse bremsstrahlung heating depends on collisional ionization, and is proportional to electron temperature, ionization potential, pulse intensity, and gas density [3]. IB heating allows for the initialization and expansion of the blast wave which shapes the waveguide. The Lorentz plasma model is used frequently to predict how different laser parameters will impact the resulting electron energy. The parameters examined here include pulse duration and pulse energy. The heating rate calculated through this model is shown in (1).

$$\frac{d\varepsilon}{dt} = \left(\frac{e^2 E_0^2}{2m_e \omega^2}\right) \left[\frac{\omega^2}{\omega^2 + v_m^2}\right] v_m \approx 2U_p v_m \tag{1}$$

In (1), ε is electron heating, t is time, e and m_e are the electron charge and mass, respectively, and v_m is the momentum-transferring collision rate. U_p is ponderomotive potential, E_0 is the electric field of the laser, and ω is the laser frequency.

A. Sedov Blastwave Expansion

As a preliminary analysis of low-density plasma waveguide behavior, we simulate a Sedov blastwave utilizing the desired experimental parameters. By solving for the blast wave expansion radius as a function of time, R(t), the blastwave density, pressure, and radial velocity can be calculated. R(t) is given by solving Eq. (2)

$$R(t) = C_{\nu}(\gamma) \left(\frac{Et^2}{\rho_0}\right)^{(1/(\nu+2))},$$
 (2)

where ρ_0 represents the initial density of the blast wave, E is the energy deposited, C_v is the specific heat, γ is the specific heat ratio, and v is a dimensionless geometry parameter, with v = 2 for our cylindrical geometry.

For ξ defined as r/R(t); r is the radius within which initial energy is deposited to form the blastwave, and R(t) is blastwave expansion radius as a function of time.

$$\rho = \rho_1 = \frac{\gamma + 1}{\gamma - 1} \rho_0 \tag{3}$$

$$\frac{\rho(\xi)}{\rho_1} \propto \xi^{\nu/(\gamma - 1)} \tag{4}$$

(3) is the analytic solution for ρ immediately after the shock front, and (4) is the solution near the center. Solutions to (3) and (4) are solved at every time step in order to get the behavior of the blast wave's density at all positions during a desired amount of time.

B. FLASH Simulations

FLASH is a hydrodynamic code which has extensive applications that encompass a wide variety of phenomena studied in physics [5]. FLASH utilizes IB energy deposition to model laser power deposition in a medium. A ray tracing algorithm is used to take into account beam propagation, and the laser power in a "cell" of the simulation is calculated using the energy from inverse bremsstrahlung.

The power deposited due to IB heating can be written as seen in (5), where P_t is the power as a function of time t, P_0 is the initial power of the system, and v_{ib} is the IB frequency.

$$P_{t} = P_{0}e^{-\int_{0}^{t} v_{ib}(t')dt'}.$$
 (5)

The momentum collision rate is explicitly given in the following form.

$$v_m = \frac{4}{3} \left(\frac{2\pi}{m_e} \right)^{\frac{1}{2}} \frac{Ze^4}{n_c k_B^{\frac{3}{2}}} \frac{n_e[r(t)]^2 \ln \Lambda[r(t)]}{T_e[r(t)]^{\frac{3}{2}}}$$
(6)

In (6), Z is the atomic number, n_e is electron density, $\ln \Lambda$ is the Coulomb logarithm, k_B is the Boltzmann constant, n_c is

critical density, electron temperature is T_e and r(t) represents a given simulated ray's position as a function of time.

r(t) is the ray position as it changes with time in the simulation, as seen in the (7) below, r_0 is the initial ray position and v_0 is the initial velocity of the ray.

$$r(t) = r_0 + v_0 t - \frac{c^2}{4n_c} \nabla n_e(r_0) t^2$$
 (7)

When the ray position equation is inserted into the inverse bremsstrahlung momentum collision rate, the end result, is

$$\int_0^t \mathbf{v}_{ib}(t')dt' = \mathbf{v}_{ib}(t) = \mathbf{v}_{ib}(0)\frac{t}{2}\sum_{i=1}^2 \omega_i \frac{(1 + Ut_i + Rt_i^2)^2}{(1 + Wt_i + St_i^2)^{3/2}}, \quad (8)$$

where

$$U = \frac{\nabla n_e(r_0) \cdot v_0}{n_e(r_0)}$$

$$W = \frac{\nabla T_e(r_0) \cdot v_0}{T_e(r_0)}$$

$$R = -\frac{c^2 \nabla n_e(r_0) \cdot \nabla n_e(r_0)}{4n_c n_e(r_0)}$$

$$S = -\frac{c^2 \nabla T_e(r_0) \cdot \nabla n_e(r_0)}{4n_c T_e(r_0)}.$$
(9)

where $v_{ib}(0)$ is the inverse bremsstrahlung frequency at t = 0. The summation index i in (8) is a result of the time having two potential values, $t_{1,2} = (1 \pm 1/\sqrt{3})t/2$, equally weighted. (8) is used at each step of the simulation and inserted into (5) which can be used to derive the IB power [5], [6].

The rays can be seen in action in Fig. 1, which shows the path of the laser in an upward vertical direction, which is a supergaussian beam and has a square pulse profile (see (10)) of duration 100 ps, and a peak intensity of $I_0 = 4.2 \times 10^{15}$ W/cm². The intensity I_{sg} of the supergaussian is written as:

$$I_{sg}(r) = I_0 \exp\left\{-\left[\left(\frac{r}{R_{sg}}\right)^2\right]^N\right\}$$
 (10)

where the beam e-folding length R_{sg} is fixed to 7.5 μ m and N=2 is used in our simulations.

In Fig. 2, the laser propagates through a Helium gas with density 2×10^{17} cm⁻³. Parameters of the gas (opacity data and equations of state) are included in the FLASH simulation and then considered as the laser heats the gas. There was an initial temperature of 290 Kelvin, the gas is then ionized as the laser intensity grows in time. It should be noted in this paper we plot our simulations in Cartesian coordinates, with z being the axis of propagation of the laser and x being the axis perpendicular to the laser propagation.

In Fig. 2 it is possible to see the electron temperature and densities characteristic of an incipient blastwave. This plot was taken immediately after the 100 ps pulse propagated through the gas. Fig. 2a shows the electron temperature in kelvin. Converting to electron volts, the maximum temperature (red)

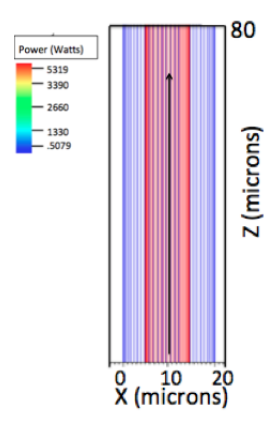


Fig. 1. Initial conditions of laser simulation (Cartesian coordinates). Path of laser through Helium gas. The laser travels through a gas with an initial helium gas density of approximately 2×10^{17} cm⁻³.

is about 129 eV. In Fig. 2b, the edges of the electron density blastwave pattern possesses a higher density than the middle, demonstrating the similarity of the behavior to a shockwave. With IB heating, longer pulses will provide even greater gas heating, resulting in higher electron temperature spikes [3].

C. Experimental Setup

As seen in Fig. 3a, we are planning to use a multiple object plane imaging system (MOPI) [7], that is more versatile than other techniques such as transverse interferometry. MOPI works by separating the probe beam into several copies after interacting with the pump beam. Each copy is imaged from a different object plane by various CCD (charge coupled device) cameras. The phase can then be reconstructed using a typical phase retrieval algorithm [8]. Fig. 3b show how the pulse width can be varied for picosecond pulses. Using the uncompressed and chirped amplified pulses of our laser to drive the blastwave, we can, for example, decrease the pulse duration on the 100-ps time scale by restricting bandwidth of the beam while it is spatially chirped between compressor prisms in the laser front-end. A key portion of our experiment is the ability to modify pulse width and find the most successful parameters to use to create waveguides at low densities.

III. OPTICAL FIELD IONIZATION

A. OFI Heating Model

In planned experiments, we will use a reflecting axicon to achieve a multi-cm line focus. OFI heating depends on pulse energy, duration, polarization and on gas species. Here we determine an explicit electron energy distribution for pulses of various durations and foci. Then, assuming a delta-function style impulse of this sudden appearance of plasma, we use a hydrodynamic code to simulate blastwave expansion.

To describe OFI heating as derived in [9], [10], we first determine an ion distribution. Here, the ion population N_i of each ionization level, i (where N_0 denotes neutral atoms) for any given ion species is given by numerically solving the coupled rate equations [11]:

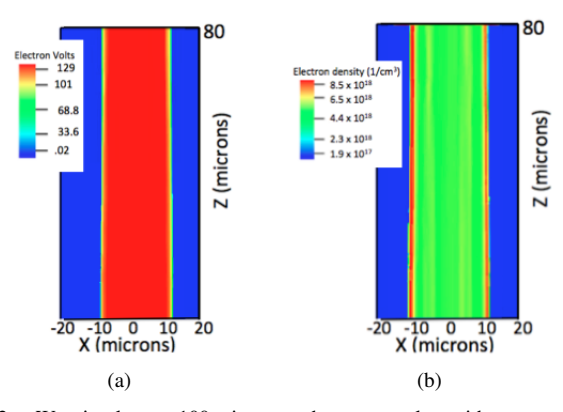


Fig. 2. We simulate a 100 picosecond square pulse with a super gaussian intensity profile (Cartesian coordinates). The pulse of intensity 4.2×10^{15} Watts/cm² was sent through a chamber of Helium with an initial density of 2×10^{17} cm⁻³. (a) Electron temperature, the maximum electron energy is approximately 129 eV. (b) Electron density after the laser pulse has propagated through the Helium gas.

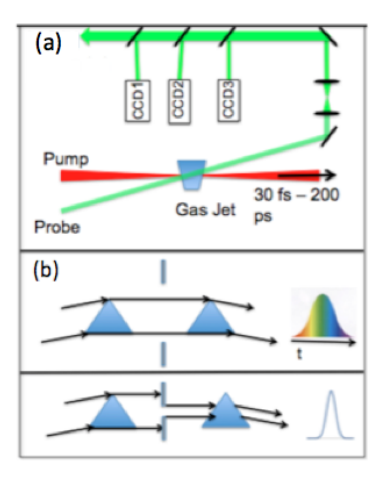


Fig. 3. MOPI imaging setup (a) which can be used at lower densities than transverse interferometry. There is an additional schematic (b) of a setup of a spatially chirped beam between two compressor prisms, allowing for modification of pulse width.

$$\frac{d}{dt}N_i = (1 - \delta_{i,0})\Gamma_{i-1}N_{i-1} - (1 - \delta_{i,Z})\Gamma_i N_i$$
 (11)

where $\delta_{i,j}$ is the Kronecker delta function, and j represents the atomic number Z (and i is the ionization level). Γ_i is the ionization rate [12], [13] (in atomic units) that describes the rate of ionization for an atom in an electric field \vec{E} and has the following form:

$$\Gamma_i = A_{n^*l^*} B_{l|m|} I_i \left(\frac{2(2I_i)^{3/2}}{|E|} \right)^{2n^* - |m| - 1} \exp\left(\frac{2(2I_i)^{3/2}}{3|E|} \right)$$
(12)

In the this equation I_i is is the ionization potential of the i^{th} ion, $n^* = Z^*/\sqrt{2I_i}$ where Z^* is the charge of the i^{th} ion, and $l^* = n_0^* - 1$ denote the effective principal quantum number and angular momentum (n_0^*) is the effective principal quantum number for the ground state). l and m denote the

angular momentum and its projection on the laser polarization direction, respectively. $A_{n^*l^*}$ and $B_{l|m|}$ are written as:

$$A_{n^*l^*} = \frac{2^{2n^*}}{n^*\Gamma(n^* + l^* + 1)\Gamma(n^* - l^*)},$$

$$B_{l|m|} = \frac{(2l+1)(l+|m|)!}{2^{|m|}|m|!(l-|m|)!},$$

here $\Gamma(x)$ is the gamma function. Next, we can describe the total electron population *S* knowing the rates of change in the ion population levels:

$$\frac{d}{dt}S = \sum_{i}^{Z} \frac{d}{dt} N_i(t) \Theta \left[\frac{d}{dt} N_i(t) \right]$$
 (13)

where Θ is the Heaviside step function that prevents electrons from being subtracted as ions are ionized to higher levels. Now with the electron population, the energy E_k that an electron acquires due to OFI heating is [10]:

$$E_k(t_i) = \frac{e^2}{2m_e} |\vec{A}(t_i)|^2$$
 (14)

In this equation e is the electron charge, m_e is the electron mass, and $\vec{A}(t_i)$ is the vector potential of the laser field at the time t_i that the electron is freed from its atom. Because the electron energy is determined only at the time at which it is ionized, we write the electron energy distribution f(E) as:

$$f(E) = \int_{-\infty}^{\infty} \delta(E - E_k(t)) \frac{d}{dt} S(t) dt$$
 (15)

where the dirac delta term takes into account the fact that electrons leave the laser pulse with a net energy equal to the energy E_k at the time t that they are ionized (here we also ignore plasma recombination). From (15) we can then write the average energy of the electron energy distribution E_{avg} as:

$$E_{avg} = \frac{1}{N_o} \int_{-\infty}^{\infty} E_k(t) \frac{d}{dt} S(t) dt$$
 (16)

where $N_e = \int_{-\infty}^{\infty} S(t) dt$ is the total number of ionized electrons. Fig. 4 shows a comparison of (15) plotted against a simulation in Smilei [11], for pulses circularly polarized, with 30 fs FWHM duration, and had a peak intensity of 5×10^{16} W/cm². The average energy found using the OFI model and (16) is 733 eV. We can see that (15) tracks the results from Smilei well.

We point out that circular polarization can in general be more efficient at heating than linearly polarized pulses [1]. For example, at the same parameters that was used to create Fig. 4, the average energy from a linearly polarized beam is 105 eV. Also, in elements with higher ionization potentials, ionization can peak around times that correspond to higher vector potentials $\vec{A}(t)$ that accelerate the ionized electrons to higher energies - see (14). Helium in particular enables generation of hotter initial plasmas (due to Helium's relatively high first and second ionization levels) while still allowing for a fully ionized blastwave. As discussed in [1], shorter pulses also lead to hotter plasmas when compared to longer pulses of the same peak intensity.

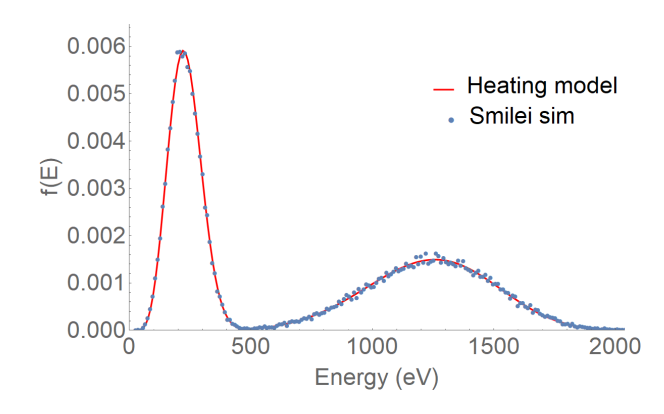


Fig. 4. Distribution of electron energies from a circularly polarized 30 fs FWHM gaussian pulse of peak intensity of 5×10^{16} W/cm² ionizing an initially neutral He gas. First peak in the distribution at 240 eV comes from ionizing He to He^{1+} and the second peak at 1270 eV comes from ionizing He^{1+} to He^{2+}

B. Axicon Blastwave Asymmetry

An axicon can generate a line focus several tens of centimeters long, making it an ideal candidate for generating long waveguides. However, spatial line focus intensity variations arising from certain axicon geometries and input beam profiles can lead to nonuniform blastwave expansion. The intensity equation for a conical axicon lens resulting from an incident Gaussian beam as a function of distance z from the axicon's position and radius r from the line focus is [14]:

$$I_{ax}(r,z) = I_0 \frac{\pi k R^2}{2z_f} \frac{z}{z_f} \exp\left[-2(zR/z_f r_0)\right] J_0 (krR/z_f)^2$$
 (17)

In this equation, k is the wavenumber, I_0 is the peak intensity of the incident gaussian beam, R is the radius of the axicon, and z_f is the line focus length. z_f is written as $z_f = R/\tan(\gamma_0) - H$ where $\gamma_0 = \sin^{-1}(n\sin(\alpha)) - \alpha$ is the convergence angle, α is the axicon base angle, n is the index of refraction of the axicon $(n \approx 1.5)$ and H is the axicon's height. J_0 is the zero-order Bessel function of the first kind.

The increase of OFI heating drops off significantly with increasing optical peak intensity once the pulse is strong enough to fully ionize the population; ionization will occur at times that correspond to approximately the same field strength - and by (14) electrons will gain the same approximate energy distribution. This happens for He at approximately I_0 more than 2×10^{16} W/cm² for an axicon with R = 7 cm, $\alpha = 30^{\circ}$, $z_f = 16.8$ cm and an input pulse fixed at 30 fs FWHM. This stable behavior could help create a more uniform blastwave - even for nonuniform intensities along the axicon line focus z_f .

We simulated variation of the initial energy deposition resulting from the intensity along the axicon line focus (centered at x=100 μ m in Fig. 5) using Mathematica [15] and (15), assuming an incident gaussian pulse with 1 J energy, 30 fs FWHM pulse duration at a wavelength of $\lambda=800$ nm. This energy density was passed in to FLASH to simulate

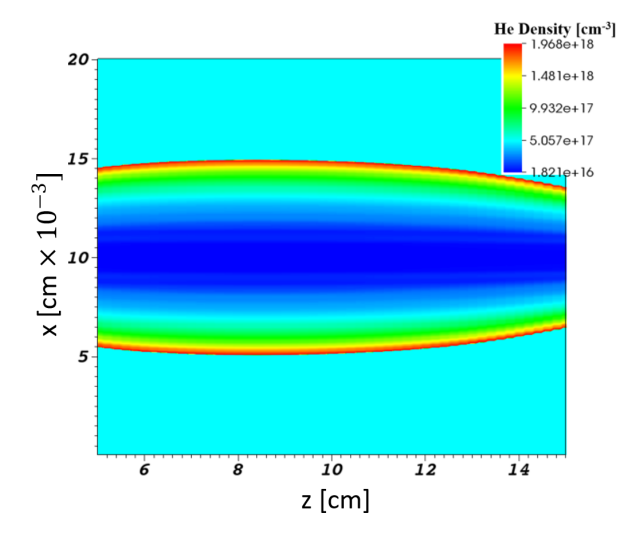


Fig. 5. Blastwave formation from an axicon line focus (Cartesian coordinates; note that z is the axis of propagation of the laser, which now propagates along the horizontal axis). Notice how the ends of the blastwave evolve slower due to the less intense beam at those locations. Color legend indicates number density of Helium ions in cm⁻³ that will be proportional to the electron density inside the shockwave. Outside the shockwave is a neutral Helium gas.

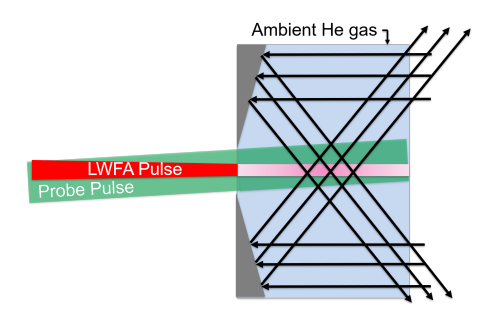


Fig. 6. OFI experimental setup. Laser wakefield accelerating pulse (LWFA) and probe pulse strike a hole in the reflecting axicon from the left, and the channel-forming pulse strikes the axicon from the right, creating the line focus that drives the plasma blastwave.

the blastwave hydrodynamic evolution using its Sedov solver; we approximated the waveguide evolution as a hydrodynamic blastwave that evolves according to the Sedov equations [16] (see Fig. 5). We see that the region for which I_0 is more than 2×10^{16} W/cm², (around z=8 cm in this scenario), the blastwave demonstrates a relatively constant expansion. The remaining non-uniformities can be reduced by adjusting the input beam spatial distribution or by modifying the axicon's surface [14].

In future work, we plan to experimentally study femtosecond-scale heating and blastwave evolution as a function of length, using a reflective axicon as shown in Fig. 6. Use of MOPI will allow us to probe and quantify how channel formation varies with distance in an axicon line focus.

IV. CONCLUSIONS

We will use modeling in the ATI and IB heating schemes to expand upon existing work and examine the efficacy of creating low density waveguides over a wide range of pulse widths. The pre-experimental work presented will be used to characterize parameters for experiments done on the UT^3 and Texas Petawatt laser systems. Simulations of both IB and OFI heating produce plasmas on the order of tens of eV (IB) to hundreds of eV (OFI), but more work is needed to evaluate the advantages and disadvantages of IB and OFI heating.

REFERENCES

- [1] N. Lemos et al., "Effects of laser polarization in the expansion of plasma waveguides," Phys. Plasmas, vol. 20, p. 103109, 2013.
- R. Shalloo et al., "Hydrodynamic optical-field-ionized plasma channels," Phys. Rev. E, vol. 97, p. 053203, 2018.
- [3] C. G. Durfee, J. Lynch, and H. M. Milchberg, "Development of a plasma waveguide for high-intensity laser pulses," Phys. Rev. E, vol. 51, pp. 2368–2389, 1995.
- [4] E. W. Gaul et al., "Production and characterization of a fully ionized he plasma channel," Appl. Phys. Lett., vol. 77, p. 4112, 2000.
- [5] FLASH Center for Computational Science, "FLASH Version 4.5," Chicago, IL, 2017.
- [6] FLASH User's Guide, FLASH Center for Computational Science, 2017.
- [7] Z. Li et al., "Single-shot visualization of evolving, light-speed structures by multiobject-plane phase-contrast imaging," Opt. Lett., vol. 38, p. 5157, 2013.
- [8] Z. Li et al., "Single-shot visualization of evolving plasma wakefields," AIP Conf. Proc., vol. 1777, p. 040010, 2016.
- [9] S. C. Rae and K. Burnett, "Possible production of cold plasmas through optical-field-induced ionization," Phys. Rev. A, vol. 46, p. 2077, 1992.
- [10] N. Lemos et al., "Plasma expansion into a waveguide created by a linearly polarized femtosecond laser pulse," Phys. Plasmas, vol. 20, p. 063102, 2013.
- [11] J. Derouillat et al., "Smilei: A collaborative, open-source, multi-purpose particle-in-cell code for plasma simulation," Comput. Phys. Commun., vol. 222, pp. 351–373, 2018.
- [12] A. M. Perelomov, V. S. Popov, and M. V. Terentev, "Ionization of atoms in an alternating electric field," Sov. Phys. JETP, vol. 23, pp. 924–934, 1966
- [13] M. V. Ammosov, N. B. Delone, and V. P. Krainov, "Tunnel ionization of complex atoms and of atomic ions in an alternating electromagnetic field," Sov. Phys. JETP, vol. 64, p. 1191, 1986.
- [14] V. V. Korobkin, L. Y. Polonski, V. P. Poponin, and L. N. Pyatnitski, "Focusing of gaussian and super-gaussian laser beams by axicons to obtain continuous laser sparks," Sov. J. Quantum Electron., vol. 16, p. 178, 1986.
- [15] Wolfram Research, Inc., "Mathematica, Version 11.2," Champaign, IL, 2017.
- [16] L. I. Sedov, Similarity and Dimensional Methods in Mechanics. New York: Academic, 1959.